Graphene Layer Growth Chemistry: Five- and Six-Member Ring Flip Reaction[†]

Russell Whitesides,[‡] Dominik Domin,[§] Romelia Salomón-Ferrer,[§,||] William A. Lester, Jr.,[§,||] and Michael Frenklach*,[‡]

Department of Mechanical Engineering, University of California at Berkeley, and Environmental Energy Technologies Division, Lawrence Berkeley National Laboratory, Berkeley, California 94720, Kenneth S. Pitzer Center for Theoretical Chemistry, Department of Chemistry, University of California at Berkeley, 6161 Etcheverry Hall # 1740, Berkeley, California 94720, and Chemical Sciences Division, Lawrence Berkeley National Laboratory, Berkeley, California 94720

Reaction pathways are presented for hydrogen-mediated isomerization of a five- and six-member carbon ring complex on the zigzag edge of a graphene layer. A new reaction sequence that reverses the orientation of the ring complex, or "flips" it, was identified. Competition between the flip reaction and the "ring separation" was examined. Ring separation is the reverse of the five- and six-member ring complex formation reaction, previously reported as "ring collision". The elementary steps of the pathways were analyzed using density functional theory (DFT). Rate coefficients were obtained by solution of the energy master equation and classical transition-state-theory utilizing the DFT energies, frequencies, and geometries. The results indicate that the flip reaction pathway dominates the separation reaction and should be competitive with other pathways important to the graphene zigzag edge growth in high-temperature environments.

I. Introduction

Graphene has recently received much attention for its novel properties[1–7] and applications[8–10] owing to its recent synthesis as a single-atom-thick crystal on substrates[1] and more recently in the free state.[11] However, even before the realization of single-layer graphene in the laboratory, interest in understanding aromatic edge chemistry, and hence graphene chemistry, has existed because of the possible application of such knowledge to carbonaceous materials such as pyrolytic graphite, fullerenes, nanotubes, interstellar dust, large polycyclic aromatic hydrocarbons (PAHs), carbon black, and combustion soot.

Mechanistically, the H abstraction/C_2H_2 addition (HACA) model[12–14] has played a key role in understanding the growth of both PAH and soot in combustion environments. The HACA model is based on a repetitive reaction sequence of two principle steps: abstraction of a hydrogen atom from the aromatic edge by a gaseous hydrogen atom, followed by addition of gaseous acetylene molecule, the most abundant product in high-temperature environments, to the formed surface radical site. Early application of this model to soot surface reactions[15] focused on the armchair edge where the edge propagates by repeated formation of six-member rings. Subsequent studies pointed to the possible importance of zigzag edge growth, formation of five-member rings, and their migration along the zigzag edge[16,17]

The overall migration transformation (eq 1) is initiated by hydrogen addition and followed by C–C homolytic cleavage, hydrogen atom migration(s), C–C bond formation, and finally


(1)
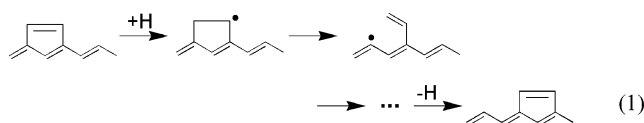
hydrogen atom loss. It was found that surface activation by hydrogen addition rather than abstraction provides a faster route for the migration isomerization.[17] The new migration phenomenon alters significantly the framework for surface chemistry of the graphene layer and introduces a large number of possible elementary reaction steps that can take place on an evolving surface. One such example is the "collision" of migrating rings examined in our prior study,[18] which results in the following overall transformation. Like the migration reaction, this trans-

(2)
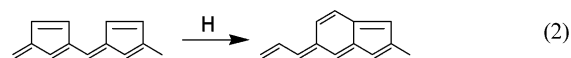
formation is initiated by hydrogen addition and is followed by a similar set of unimolecular reactions. Reaction rates of the pathway in eq 2 were found to be comparable to those of the migration reaction (eq 1).

In considering the fate of the five- and six-member ring complex produced by the collision reaction, the product of reaction 2, we have identified a new reaction possibility in which the two surface rings reverse orientation, or "flip". We report

(3)
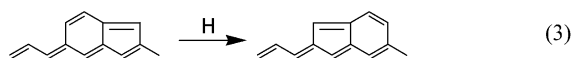
two pathways for this flip rearrangement, one initiated by hydrogen atom addition and another by hydrogen atom abstraction. The flip reaction competes directly with the reverse of the collision reaction, which we term "ring separation". Here we present results of quantum-chemical and reaction rate analyses of these two competing reactions. We also re-evaluate the rate of the collision reaction based on new quantum-chemical results.
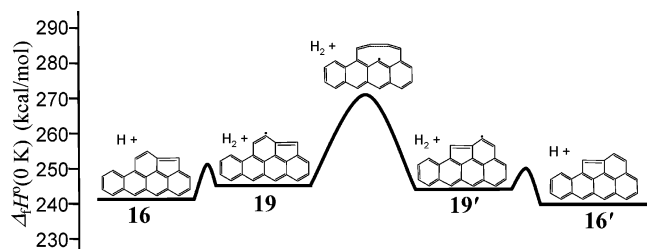
Figure 1. Potential energy diagram for the flip reaction by the H abstraction route calculated at the B3LYP/6-311G(d,p) level of quantum theory.

Finally, we evaluate the relative roles of these reactions in the framework of graphene layer chemistry.

II. Computational Details

Density functional theory (DFT) was used to calculate the molecular and energetic parameters of all stable species and transition states involved in the ring flip reaction sequences. Our process for identifying and characterizing species is similar to that employed previously for the collision reaction pathway.[18] Geometry optimizations were performed with the B3LYP hybrid functional[19] and the 6-311G(d,p) basis set. Previous studies have shown energetic predictions of B3LYP calculations at the 6-311G(d,p) level to be in good agreement with experimental and high-level ab initio results for stable species.[20−22] The energies of transition states predicted by this method, however, are often underestimated by about 5 kcal mol^{-1}.[23,24] This shortcoming lessens the accuracy of rate coefficients derived from the calculated energetics yet allows for an order-of-magnitude analysis, thus satisfying the objective of the present study. The substrate used for the calculations is tetracene, the smallest linear aromatic molecule (oligoacene) on which the collision reaction (eq 2) can occur, thus minimizing the computational expense of the quantum-chemical calculations.

Vibrational analysis was performed at each predicted stationary point to confirm the point to be an energetic minimum (no imaginary frequencies) or a saddle point (one imaginary frequency). Transition states were confirmed to connect the reactant and product stable species by visual inspection of normal modes corresponding to the imaginary frequencies calculated at the B3LYP/6-311G(d,p) level and by intrinsic reaction coordinate calculations at the B3LYP/3-21G level.
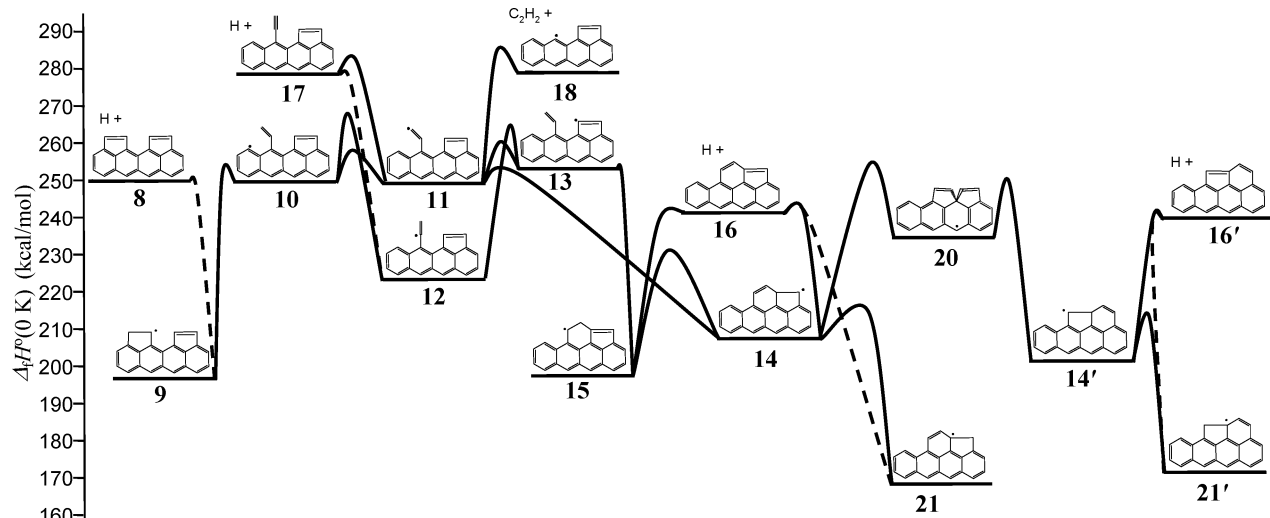
Zero-point energies were determined from the force calculations and scaled by a factor of 0.9668.[25] All calculations were performed using the Gaussian 03 suite of codes[26] on an Intel Xeon cluster.

Chemical-activation and transition-state-theory rate coefficients for the reactions were determined using version 2.08 of the MultiWell suite of codes.[27,28] MultiWell employs a stochastic approach to solution of the master equations for energy transfer in unimolecular reaction systems.[27,29] Microcanonical rate coefficients for the elementary reactions of these models were calculated with MultiWell at the RRKM level of theory.

The key inputs to MultiWell—reaction barriers, frequencies, and moments of inertia—were assigned from the DFT calculations at the B3LYP/6-311G(d,p) level of the present study. Following Gilbert and Smith[30] the real frequencies below 150 cm^{-1} were examined by graphically visualizing the associated normal mode vibrations to identify internal rotational modes. Only species already identified in our previous study on the collision pathway[18] were found to exhibit internal rotations. Some of those species were found to have both a one-dimensional (1D) rotation and a two-dimensional precession rotation of a C_2H_x moiety. These internal rotations were treated as free rotors with one harmonic frequency being removed from the density of states calculations for each rotor dimension as identified by the graphical visualization. For both rotations, we took the moment of inertia to be that of the 1D rotor calculated for the axis containing the twisting bond. Sensitivity of the rate coefficient calculations to internal rotational modeling was tested previously,[18] and we found no measurable deviation in the results with rotational treatment ranging from the harmonic oscillator approximation to that of the free rotor. See the Supporting Information for internal rotor moments of inertia as well as other pertinent molecular parameters.

The sums and densities of states for intermediate species and transition states were determined by exact count with a grain size of 10 cm^{-1}, maximum energy of 500 000 cm^{-1}, and the dividing level between the high- and low-energy regimes set at 2500 cm^{-1}. Lennard-Jones parameters for the reactants and intermediates were taken from an empirical correlation.[31] Argon was chosen as the bath gas collider. The collisional energy transfer was treated by the exponential-down model with $\langle \Delta E_{down} \rangle = 260$ cm^{-1} based on the data of Hippler et al.[32]

Figure 2. Potential energy diagram for the combined collision reaction and flip reaction by the H addition route calculated at the B3LYP/6-311G-(d,p) level of quantum theory.

Graphene Layer Growth Chemistry

J. Phys. Chem. A, Vol. 112, No. 10, 2008 **2127**

TABLE 1: Comparison of Equilibrium Constant (K_{eq}) and Rate Coefficient (k) of H Abstraction Reactions for Benzene (per Site)[15,33,34] and for Species 16

T (K)	K_{eq}	k (10^{12} cm^3 mol^{-1} s^{-1})			K_{eq}	k (10^{12} cm^3 mol^{-1} s^{-1})
	a	b	c	a	a	a
1500	1.83	0.195	0.665	2.44	3.06	3.80
1750	2.31	0.420	1.65	5.22	3.64	7.85
2000	2.69	0.746	3.33	9.53	4.07	13.9
2250	2.99	1.17	5.87	15.6	4.38	22.3
2500	3.21	1.67	9.37	23.5	4.58	33.1

[a] Present work; calculated from partition functions and transition state theory, based on molecular parameters from B3LYP/6-311G(d,p) calculations. [b] Taken from ref 33. [c] Calculated from the reverse reaction rate coefficient, taken from ref 34, multiplied by K_{eq} from the present work.

MultiWell simulations were performed for temperatures ranging from 1500 to 2500 K and pressures from 0.1 to 10 atm. The numerical runs were carried out for reaction times ranging from 1×10^{-11} to 1×10^{-2} s. For each set of conditions, between 10^6 and 10^7 stochastic trials were performed to maintain statistical error in species fractions used to derive rate coefficients of less than 10%.

III. Results and Discussion

Potential Energy Calculations. Our potential energy surface (PES) calculations revealed two pathways for the ring flip reaction (eq 3). The first possibility is one initiated by hydrogen abstraction from the reactant molecule whose PES is shown in Figure 1.

The other flip reaction pathway that we have identified is initiated by hydrogen addition to the reactant molecule. This pathway turned out to be much slower than the abstraction pathway. However, because of its overlap with the collision reaction pathway, we included the new species in the calculations of rate coefficients for the collision and separation reactions. The combined PES for the collision reaction and the flip pathway initiated by hydrogen addition is shown in Figure 2. Species **8**−**16** and transition states connecting them (except the transition state connecting species **14** and **15**) comprise the mechanism for collision that was examined in our previous work,[18] and the numbering of species remains consistent. Species **9**−**15**, **14′**, **20**, **21**, and **21′** are all isomers of the C$_{22}$H$_{13}$ radical and, along with the transition states that connect them, make up a unimolecular reaction system connecting the various product sets, namely, **8**, **16**, **16′**, **17**, and **18**. For example, the reaction **8** + H → **16** + H is the collision reaction and **16** + H → **16′** + H is the flip reaction. In addition, **8** + H can react directly to **16′** + H without having to pass through species **16**. We were unable to locate transition states connecting species **21** to **16** and **21′** to **16′** because of the flat shape of the PES at still large H−C distances. Molecular parameters (geometries, frequencies, and energies) for these transition states were taken from the similar transition states, **14**−**16** and **14′**−**16′**. Similarly, transition states connecting species **8**−**9** and **12**−**17** were not found at the B3LYP/6-311G(d,p) level. Geometries and frequencies for these transition states were taken from B3LYP/3-21G calculations, and barriers of 0.5 kcal mol^{-1} with respect to **8** + H and **17** + H were assumed. Transition states not found at the B3LYP/6-311G(d,p) level are shown as dashed lines in Figure 2.

Reaction Rates. The reaction system **16** + H → **19** + H$_2$, **19** → **19′**, and **19′** + H$_2$ → **16′** + H is depicted in Figure 1. It
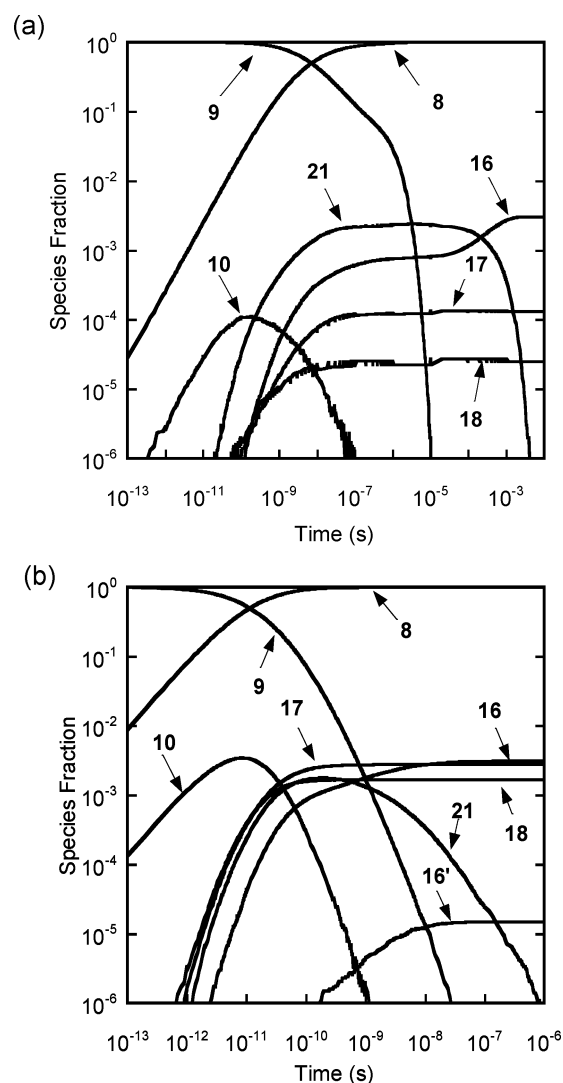
Figure 3. Species fractions as a function of reaction time for chemical-activation reaction **8** + H → **9** → products at 1 atm and (a) 1500 and (b) 2500 K.

was modeled as a three-step process: (a) bimolecular reaction forming **19** by hydrogen abstraction from **16**, (b) unimolecular transformation of the radical intermediate, **19** → **19′**, and (c) bimolecular reaction of **19′** with H$_2$ to form **16′**. The rate of the unimolecular transformation, step b, was found to be on the order of 10^{10}−10^{11} s^{-1} between 1500 and 2500 K. Considering that the rate of abstraction, step a, is on the order of 10^{12}−10^{13} [H] cm^3 mol^{-1} s^{-1} for the same temperature range, the
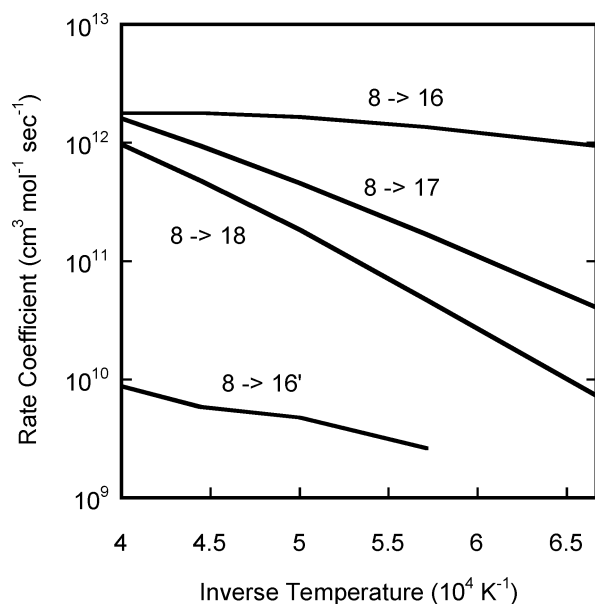
Figure 4. Rate coefficients for chemical-activation reaction $8 + H \rightarrow 9 \rightarrow$ products as a function of inverse temperature at 1 atm.

Figure 5. Rate coefficients for chemical-activation reaction $16 + H \rightarrow 14/15/21 \rightarrow$ products as a function of inverse temperature at 1 atm.

abstraction step will be rate-determining even for very large mole fractions of hydrogen atoms. For example, even for unrealistically high mole fraction of 0.1, at 10 atm and 1500 K, the species concentration of hydrogen is 8×10^{-6} mol cm^3. As a result, fast interconversion will create partial equilibrium between species **19** and **19′**. The radical can then react with H$_2$ either back to the initial species, **16**, or forward to the flipped species, **16′**, with equal probability (for a symmetric substrate). Therefore, the rate for the overall flip abstraction pathway can be assumed to be half of the hydrogen abstraction rate. In Table 1, we present the rate coefficient for the H abstraction reaction and compare it and the corresponding equilibrium constant with those of hydrogen abstraction from benzene.[15,33,34]

Reaction rate coefficients for the updated collision reaction, the separation reaction, and the flip reaction via the hydrogen addition route were calculated by a standard chemical-activation mechanism.[30,35] Due to the presence of species with high energetic stability (50 kcal mol^{-1} or more) with respect to other species on the pathway, these reactions are slow to reach equilibrium. At 1500 K, these reactions can take as long as 10 ms to equilibrate, and therefore the intermediates might react with gaseous species before unimolecular decomposition. For instance, stable species **9**, **15**, **21**, and **21′** could undergo hydrogen abstraction by gaseous radicals forming the same graphene product as would hydrogen elimination by unimolecular decomposition. The slow time evolution of this system is exemplified in Figure 3 for the $8 + H \rightarrow 9 \rightarrow$ products reaction at both 1500 and 2500 K.

We used product species fractions from the fully evolved systems to calculate the chemical-activation rate coefficients for the reactions $8 + H \rightarrow 9 \rightarrow$ products and $16 + H \rightarrow 14/15/21 \rightarrow$ products, and these results are shown in Figures 4 and 5. The difference between taking the fully equilibrated species fractions and those, say, at 10^{-6} s is only significant at lower temperatures, and even then the difference is no larger than a factor of 5 (Figure 3). For the reaction originating from species **16**, there are three inlet channels, $16 + H \rightarrow 14$, $16 + H \rightarrow 15$, and $16 + H \rightarrow 21$, and the rate coefficients shown in Figure 5 for the overall reactions were calculated as the sum of the respective rate coefficients.
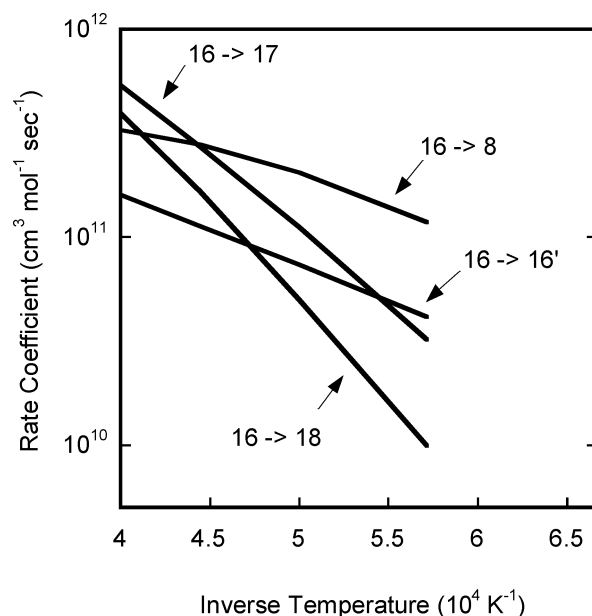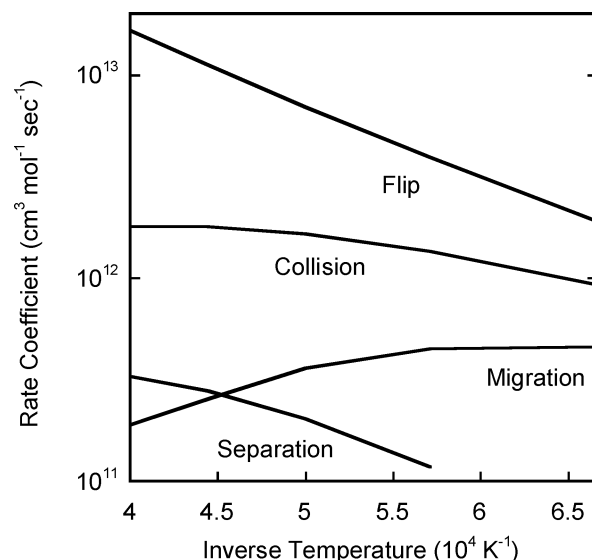

Figure 6. Comparison of rate coefficients of the flip (both the addition and the abstraction channels), collision, separation, and migration[18] reactions.

The reported chemical-activation rate coefficients are for pressures of 1 atm. No measurable deviations in the calculated rate coefficients were obtained with changing pressure from 0.1 to 10 atm. For a few of the reaction channels, we were unable to calculate species fractions with statistical accuracy at 1500 K, due to computational expense or limitations of the stochastic code, and hence these data points are missing in Figures 4−6. The recomputed rate coefficient for the collision reaction is decreased from that previously reported[18] by a factor of about 1.5 at 1500 K and 3 at 2500 K, which is mainly due to the inclusion of products **17** and **18** as competing channels but not due to the addition of the flip reaction channel species.

Finally, we compare the overall rate coefficients for migration, collision, separation, and the flip reaction in Figure 6. Inspection of the results indicates that the rate of the flip reaction is on the same order of magnitude and faster than those for the collision and migration reactions and dominates the ring separation
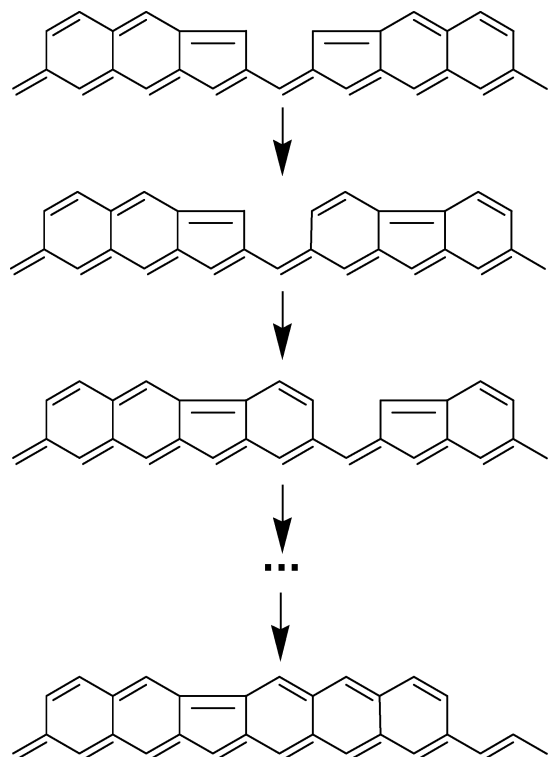
Figure 7. Successive ring flip reactions leading to a decrease in five-member rings on the graphene surface.

reaction. This fast reaction rate means that in evolving graphene layers flipping of the complex formed by the collision reaction will occur much more rapidly than the ring separation reaction and on the same time scale and faster than collision and migration, which have been previously reported as predominant reactions on the zigzag edge.[17,18]

IV. Conclusions

A new reaction pathway was identified, which reverses orientation of the five- and six-member carbon ring complex on a graphene zigzag edge, a "flip" transformation. The analysis of the flip reaction indicates that it occurs with rates comparable to and exceeding those of the migration and collision reactions, with the latter reactions suggested to play an important role in graphene zigzag edge chemistry in high-temperature environments.[18] In addition, the flip reaction is orders of magnitude faster than the ring separation reaction, with which it directly competes.

The new reaction adds an important step in graphene layer growth. Among other things, it suggests the possibility of a five-member ring traveling through a row of six-member rings such as

(4)
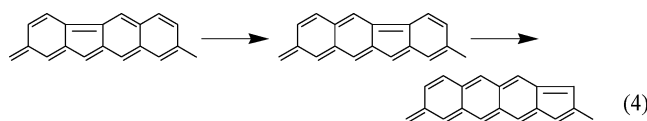
The rate of such reactions will influence the number and location of five-member rings that are incorporated into growing graphene layers (Figure 7) and hence will significantly affect the resulting morphology.

Supporting Information Available: Molecular parameters for all species including atomic coordinates, energies, harmonic frequencies, and internal rotor moments of inertia. This material is available free of charge via the Internet at http://pubs.acs.org.

References and Notes

(1) Novoselov, K. S.; Geim, A. K.; Morozov, S. V.; Jiang, D.; Zhang, Y.; Dubonos, S. V.; Grigorieva, I. V.; Firsov, A. A. *Science* **2004**, *306*, 666.

(2) Berger, C.; Song, Z.; Li, X.; Wu, X.; Brown, N.; Naud, C.; Mayou, D.; Li, T.; Hass, J.; Marchenkov, A. N.; Conrad, E. H.; First, P. N.; de Heer, W. A. *Science* **2006**, *312*, 1191.

(3) Heersche, H. B.; Jarillo-Herrero, P.; Oostinga, J. B.; Vandersypen, L. M. K.; Morpurgo, A. F. *Nature* **2007**, *446*, 56.

(4) Ohta, T.; Bostwick, A.; Seyller, T.; Horn, K.; Rotenberg, E. *Science* **2006**, *313*, 951.

(5) Son, Y.-W.; Cohen, M. L.; Louie, S. G. *Nature* **2006**, *444*, 347.

(6) Zhang, Y.; Tan, Y.-W.; Stormer, H. L.; Kim, P. *Nature* **2005**, *438*, 201.

(7) Novoselov, K. S.; Geim, A. K.; Morozov, S. V.; Jiang, D.; Katsnelson, M. I.; Grigorieva, I. V.; Dubonos, S. V.; Firsov, A. A. *Nature* **2005**, *438*, 197.

(8) Van Noorden, R. *Nature* **2006**, *442*, 228.

(9) Stankovich, S.; Dikin, D. A.; Dommett, G. H. B.; Kohlhaas, K. M.; Zimney, E. J.; Stach, E. A.; Piner, R. D.; Nguyen, S. T.; Ruoff, R. S. *Nature* **2006**, *442*, 282.

(10) Cheianov, V. V.; Fal'ko, V.; Altshuler, B. L. *Science* **2007**, *315*, 1252.

(11) Meyer, J. C.; Geim, A. K.; Katsnelson, M. I.; Novoselov, K. S.; Booth, T. J.; Roth, S. *Nature* **2007**, *446*, 60.

(12) Frenklach, M.; Clary, D. W.; Gardiner, W. C., Jr.; Stein, S. E. *Proc. Combust. Inst.* **1985**, *20*, 887.

(13) Frenklach, M.; Wang, H. *Proc. Combust. Inst.* **1991**, *23*, 1559.

(14) Frenklach, M. *Phys. Chem. Chem. Phys.* **2002**, *4*, 2028.

(15) Frenklach, M. *Proc. Combust. Inst.* **1996**, *26*, 2285.

(16) Frenklach, M.; Moriarty, N. W.; Brown, N. J. *Proc. Combust. Inst.* **1998**, *27*, 1655.

(17) Frenklach, M.; Schuetz, C. A.; Ping, J. *Proc. Combust. Inst.* **2005**, *30*, 1389.

(18) Whitesides, R.; Kollias, A. C.; Domin, D.; Lester, W. A., Jr.; Frenklach, M. *Proc. Combust. Inst.* **2007**, *31*, 539.

(19) Becke, A. D. *J. Chem. Phys.* **1993**, *98*, 5648.

(20) Moriarty, N. W.; Brown, N. J.; Frenklach, M. *J. Phys. Chem. A* **1999**, *103*, 7127.

(21) Nimlos, M. R.; Filley, J.; McKinnon, J. T. *J. Phys. Chem. A* **2005**, *109*, 9896.

(22) Cioslowski, J.; Piskorz, P.; Moncrieff, D. *J. Am. Chem. Soc.* **1998**, *120*, 1695.

(23) Durant, J. L. *Chem. Phys. Lett.* **1996**, *256*, 595.

(24) Heuts, J. P. A.; Gilbert, R. G.; Radom, L. *J. Phys. Chem.* **1996**, *100*, 18997.

(25) *NIST Computational Chemistry Comparison and Benchmark Database*, release 12; Johnson, R. D., III, Ed.; NIST Standard Reference Database 101; National Institute of Standards and Technology: Gaithersburg, MD, 2005.

(26) Frisch, M. J.; Trucks, G. W.; Schlegel, H. B.; Scuseria, G. E.; Robb, M. A.; Cheeseman, J. R.; J. A. Montgomery, J.; Vreven, T.; Kudin, K. N.; Burant, J. C.; Millam, J. M.; Iyengar, S. S.; Tomasi, J.; Barone, V.; Mennucci, B.; Cossi, M.; Scalmani, G.; Rega, N.; Petersson, G. A.; Nakatsuji, H.; Hada, M.; Ehara, M.; Toyota, K.; Fukuda, R.; Hasegawa, J.; Ishida, M.; Nakajima, T.; Honda, Y.; Kitao, O.; Nakai, H.; Klene, M.; Li, X.; Knox, J. E.; Hratchian, H. P.; Cross, J. B.; Bakken, V.; Adamo, C.; Jaramillo, J.; Gomperts, R.; Stratmann, R. E.; Yazyev, O.; Austin, A. J.; Cammi, R.; Pomelli, C.; Ochterski, J. W.; Ayala, P. Y.; Morokuma, K.; Voth, G. A.; Salvador, P.; Dannenberg, J. J.; Zakrzewski, V. G.; Dapprich, S.; Daniels, A. D.; Strain, M. C.; Farkas, O.; Malick, D. K.; Rabuck, A. D.; Raghavachari, K.; Foresman, J. B.; Ortiz, J. V.; Cui, Q.; Baboul, A.

G.; Clifford, S.; Cioslowski, J.; Stefanov, B. B.; Liu, G.; Liashenko, A.; Piskorz, P.; Komaromi, I.; Martin, R. L.; Fox, D. J.; Keith, T.; Al-Laham, M. A.; Peng, C. Y.; Nanayakkara, A.; Challacombe, M.; Gill, P. M. W.; Johnson, B.; Chen, W.; Wong, M. W.; Gonzalez, C.; Pople, J. A. *Gaussian 03*, revision C.02; Gaussian, Inc.: Wallingford, CT, 2004.

(27) Barker, J. R. *Int. J. Chem. Kinet.* **2001**, *33*, 232.

(28) MultiWell-2.08 Software, 2007, designed and maintained by John R. Barker with contributions from Nicholas F. Ortiz, Jack M. Preses, Lawrence L. Lohr, Andrea Maranzana, and Philip J. Stimac; University of Michigan, Ann Arbor, MI; http//aoss.engin.umich.edu/multiwell/.

(29) Barker, J. R.; Yoder, L. M.; King, K. D. *J. Phys. Chem. A* **2001**, *105*, 796.

(30) Gilbert, R. G.; Smith, S. C. *Theory of Unimolecular and Recombination Reactions*; Blackwell-Scientific: Oxford, U. K., 1990.

(31) Wang, H.; Frenklach, M. *Combust. Flame* **1994**, *96*, 163.

(32) Hippler, H.; Troe, J.; Wendelken, H. J. *J. Chem. Phys.* **1983**, *78*, 6709.

(33) Kiefer, J. H.; Mizerka, L. J.; Patel, M. R.; Wei, H. C. *J. Phys. Chem.* **1985**, *89*, 2013.

(34) Mebel, A. M.; Lin, M. C.; Yu, T.; Morokuma, K. *J. Phys. Chem. A* **1997**, *101*, 3189.

(35) Steinfeld, J. I.; Francisco, J. S.; Hase, W. L. *Chemical Kinetics and Dynamics*; Prentice Hall: Englewood Cliffs, NJ, 1999.